HAL open science

Cytotoxic anti-circumsporozoite antibodies target malaria sporozoites in the host skin

Eduardo Aliprandini, Joana Tavares, Raquel Hoffmann Panatieri, Sabine Thiberge, Marcio Massao Yamamoto, Olivier Silvie, Tomoko Ishino, Masao Yuda, Sylvie Dartevelle, François Traincard, et al.

To cite this version:

Eduardo Aliprandini, Joana Tavares, Raquel Hoffmann Panatieri, Sabine Thiberge, Marcio Massao Yamamoto, et al.. Cytotoxic anti-circumsporozoite antibodies target malaria sporozoites in the host skin. Nature Microbiology, 2018, 3 (11), pp.1224-1233. 10.1038/s41564-018-0254-z . pasteur-02425448

HAL Id: pasteur-02425448

https://pasteur.hal.science/pasteur-02425448v1

Submitted on 1 Mar 2023

HAL is a multi-disciplinary open access archive for the deposit and dissemination of scientific research documents, whether they are published or not. The documents may come from teaching and research institutions in France or abroad, or from public or private research centers.

L'archive ouverte pluridisciplinaire **HAL**, est destinée au dépôt et à la diffusion de documents scientifiques de niveau recherche, publiés ou non, émanant des établissements d'enseignement et de recherche français ou étrangers, des laboratoires publics ou privés.

Distributed under a Creative Commons Attribution 4.0 International License

Cytotoxic anti-circumsporozoite antibodies target malaria sporozoites in the host skin

Eduardo Aliprandini[a], Joana Tavares[b,c], Raquel Hoffmann Panatieri[a,d], Sabine Thiberge[a,e], Marcio Massao Yamamoto[d], Olivier Silvie[f], Tomoko Ishino[g], Masao Yuda[h], Sylvie Dartevelle[i], François Traincard[i], Silvia Beatriz Boscardin[d]*, Rogerio Amino[a]*.

[a] Unit of Malaria Infection & Immunity, Institut Pasteur, Paris, 75015, France.

[b] i3S – Instituto de Investigação e Inovação em Saúde, Universidade do Porto, Portugal.

[c] IBMC – Instituto de Biologia Molecular e Celular, Universidade do Porto, Portugal.

[d] Parasitology Department, Institute of Biomedical Sciences, University of São Paulo, 05508-000, Brazil

[e]Centre de Production et d'Infection des Anophèles, Institut Pasteur, Paris, 75015, France.

[f] Sorbonne Université, INSERM, CNRS, Centre d'Immunologie et des Maladies Infectieuses, CIMI, Paris, 75013, France.

[g] Department of Molecular Parasitology, Ehime University, Ehime, 791-0295, Japan.

[h]Department of Medical Zoology, Mie University School of Medicine, Mie, 514-8507, Japan

[i]Plateforme d'Ingénierie des Anticorps, Institut Pasteur, Paris, 75015, France

*Correspondence to roti@pasteur.fr, sbboscardin@usp.br

The circumsporozoite protein (CSP) is the major surface protein of malaria sporozoites (SPZs), the motile and invasive parasite stage inoculated in the host skin by infected mosquitoes. Antibodies against the central CSP repeats of different plasmodial species are known to block SPZ infectivity[1-5], but the precise mechanism by which these effectors operate is not completely understood. Here, using a rodent *Plasmodium yoelii* (Py) malaria model, we show that sterile protection mediated by anti-PyCSP humoral immunity depends on the parasite inoculation into the host skin, where antibodies inhibit motility and kill PySPZs via a characteristic dotty death phenotype. Passive transfer of an anti-repeats monoclonal antibody (mAb) recapitulates the skin inoculation-dependent protection, in a complement- and FcRγ-independent manner. This purified mAb also decreases motility and, notably, induces the dotty death of PySPZs *in vitro*. Cytotoxicity is species-transcendent since cognate anti-CSP repeats mAbs also kill *P. berghei* (Pb) and *P. falciparum* (Pf) SPZs. MAb cytotoxicity requires the actomyosin motor-dependent translocation and stripping of the protective CSP surface coat, rendering the parasite membrane susceptible to the SPZ pore-forming like protein secreted to wound and traverse host cell membranes[6]. The loss of SPZ fitness caused by anti-PyCSP repeats antibodies is thus a dynamic process initiated in the host skin where SPZs either stop moving[7], or migrate and traverse cells to progress through the host tissues[7-9] at the eventual expense of their own life. (228)

The CSP forms a dense-coat on the SPZ surface, being essential for the development of nascent SPZs in the mosquito midgut[10]. The protein binds to sulphated glycoconjugates *in vitro*[11] and to mosquito salivary glands and hepatocytes *in vivo*[12,13], indicating a possible role in the process of arrest and subsequent invasion of these organs/cells by SPZs[14]. The structural organization of CSP is conserved among plasmodial species and consists of a N-terminal (NT) region containing a proteolytical cleavage site sequence, a variable central repetitive region, and a C-terminal (CT) region containing a thrombospondin-like type-1 repeat domain. The ensemble of these three regions is flanked by hydrophobic amino acid sequences, characteristic of glycophosphatidylinositol (GPI)-anchored proteins[15] (Fig. 1a). The central repetitive domain and the CT region constitute the basis for the most advanced malaria vaccine candidate, RTS,S/AS01, which partially protects humans against malaria[16], presumably via high levels of anti-PfCSP repeats antibodies[17]. Indeed, mAbs targeting the CSP central repeats are known to immobilize SPZs and inhibit their infectivity both *in vitro*[18-20] and *in vivo*[1-5,7]. Accordingly, human, monkey and rodent-infecting SPZs lose their *in vivo* infectivity following pre-incubation with anti-CSP mAbs[1-3] or when intravenously (iv) inoculated into passively immunized hosts[4,5,21]. In this case, protection relies on the amount and specificity of transferred mAbs[21-24] as well as on the effective number of infectious SPZs inoculated, which depends on the host susceptibility to SPZ infection and the total number of injected parasites[5,21,22,25]. Intriguingly, several CSP-based immunization protocols failed to protect immunized hosts despite eliciting high levels of anti-CSP antibodies[26-28]. To better understand how protective antibodies target SPZs *in vivo* and in physiological conditions, we used a rodent malaria model in which BALB/c mice are extremely susceptible to PySPZ infection[29], and thus, difficult to sterile protect following CSP immunization[5,26]. Using a recombinant $PyCSP_{23-346}$ (PyCSP; Fig. 1a) and the double stranded RNA Poly I:C as adjuvant (A), we developed an immunization protocol (Fig. 1b) that efficiently protects the host following the microinjection of 5,000 PySPZs in the mouse footpad (skin). Accordingly, no detectable parasite infection in the liver (Fig. 1c) or in the blood (Fig. 1c-e) is observed following PySPZ challenge. Most importantly, immunized hosts are also completely

protected against PySPZ infection initiated by natural transmission using mosquito bites (Fig. 1d, bite). No protection, however, is observed when PySPZs are iv administered (Fig. 1d, iv). Intravascular SPZ inoculation shortcuts the skin phase of the infection, where a substantial part of the parasite population commits to invade either the lymphatics[8] or skin cells[30], and thus cannot infect hepatocytes. Consequently, inoculation with the same number of SPZs by the iv route results in higher hepatic infection than skin inoculation. To discard a possible confounding effect of dose in protection, we adjusted the number of PySPZs inoculated iv or in the skin to achieve the same level of hepatic and blood infection (Supplementary Fig. 1a,c; 2,500 SPZ iv ~ 5,000 SPZ skin). Since no protection is observed after iv challenge with the adjusted dose (Supplementary Fig. 1b), these results indicate that in this model, protective effectors target extravascular PySPZs delivered in the skin of the immune host by mosquito bite or microinjection. To identify the nature of these protective effectors, mAb-mediated depletion of $CD8^+$, $CD4^+$ and $Ly6G^+$ cells was performed in immunized hosts just prior to challenge. Despite the depletion of most targeted cells from the peripheral blood, none of these treatments revert the protection induced by the PyCSP immunization (Supplementary Fig. 2a-d). In contrast, mice lacking functional B-cells due to a mutation of the gene coding for the heavy chain-joining region ($JHT^{-/-}$) completely lose PyCSP-induced sterile protection (Fig. 1e). In addition, sera transfer from immune hosts to naïve recipients protects passively immunized animals against a PySPZ skin challenge (Supplementary Fig. 2e). Altogether, these results imply a protective action of neutralizing antibodies in the skin of the sterile protected host.

To observe the protective activity of these antibodies *in situ*, we imaged GFP-expressing PySPZs in the skin of control (A) and immune hosts (A.CSP) using high-speed spinning disk confocal microscopy. *In vivo* imaging revealed two major differences between these two groups. The first is a prominent decrease in the speed of parasites microinjected in the dermis of immune hosts (Fig. 2ab). In contrast to what was previously described using irradiated PbSPZ immunization or passive transfer of anti-PbCSP mAb[7], PySPZs were not completely immobilized in the dermis,

possibly, reflecting differences in the experimental settings, or in the availability or binding capacities of cutaneous antibodies. The second difference is the striking death of PySPZs, substantiated by the sudden loss of parasite fluorescence in the dermis of immune animals (Fig. 2c). This death process produces a peculiar fluorescent dot in the posterior end of slow-moving parasites that can be short-lived or persist for several minutes (Fig. 2c, arrowheads, left or right panels, respectively). This dotty death phenotype is observed in ~50% of the population analysed during thirty minutes after skin microinjection (Fig. 2d). Despite the decrease in speed, and the high percentage of dotty death, PySPZs are still capable of invading blood vessels (Fig. 2e, intravasation). These results indicate that migration through the skin of immunized mice is a harmful process, eventually leading to the death of most PySPZs. Those that escape killing in the dermis by invading a blood vessel cannot establish a successful infection, evidencing a loss of fitness during this deleterious progression, as supported by the decrease of parasite velocity in the skin. This loss of fitness likely results in the impairment of liver invasion and/or intrahepatic development.

Using this immunization protocol, a library of anti-PyCSP mAbs was generated to identify clonal effectors capable of sterilizing infection initiated by the skin microinjection of 5,000 PySPZs, one day after the passive transfer of 100 μg of the purified antibody. Out of the six mAbs tested, three targeting the NT region and three the repetitive region of PyCSP, only the anti-repeats J6 mAb (IgG1) completely blocked PySPZ infection (Fig. 3a). The non-protective anti-NT W24 mAb (IgG1) was used as an isotype control in the following experiments. In general, anti-NT mAbs are less effective to inhibit SPZ invasion than anti-repeats mAbs[31,32]. An exception is the anti-NT 5D5 mAb that when administered iv at high dose (300 μg) and prior to intravascular SPZ challenge, protects mice better, but not sterilely, when compared to the anti-repeats 2A10 mAb[33]. The J6 mAb remarkably recapitulates the protection observed using the sterilizing PyCSP-immunization protocol. Therefore, no protection is observed after challenge using the adjusted iv dose of 2,500 PySPZs, but sterilizing protection is obtained after skin inoculation with 5,000

PySPZs (Fig. 3b; iv and skin). The same pattern of sterile protection is also observed using ten times less PySPZs in the challenge (Supplementary Fig. 3ab). Critically, J6 also completely blocks infection initiated by the bites of infected mosquitoes (Fig. 3b, bite), corroborating that protective antibodies target extravascular PySPZs delivered in the skin. J6 protective activity is independent of the presence of the C3 protein, required for the classical, lectin and alternative complement activation pathways[34] (Fig. 3c), and of the Fc Receptor gamma (FcRγ), required for antibody-dependent phagocytosis and cell-mediated cytotoxicity[35] (Fig. 3d). *In vitro*, J6 decreases PySPZ speed in a dose-dependent manner, reaching the level of motility inhibition observed *in vivo* (Fig. 3e and 2b). More dramatically and unique, the purified mAb directly kills PySPZs, leading to the incorporation of the live cell-impermeant dye, propidium iodide (PI), into the nucleic acids of the parasite. The loss of selective membrane permeability starts at the anterior pole of PySPZs and the staining propagates towards the posterior end of the parasite (Fig. 3f, red arrowheads). PI incorporation is accompanied by the loss of GFP fluorescence, which notably recapitulates the dotty death phenotype observed *in vivo* (Fig. 3f, white arrowheads). A flow-cytometric assay was developed to detect this cytotoxic activity based on the quantification of live (GFP+/PI-) and dead (GFP-/PI+) SPZ population after 45 minutes of incubation at 37 °C (Supplementary Fig. 3cd). Fifteen anti-PyCSP mAbs were screened for their killing capacity using this method. Six of these mAbs recognize the PyCSP repeats and nine, the NT of the protein as determined by ELISA (Supplementary Table 1). However, only the two anti-repeats mAbs, J6 and 15D7, which bind to the PyCSP major repeats (QGPGAP) and strongly label live PySPZs, are cytotoxic *in vitro* and confer sterile protection *in vivo* (Fig. 3a,g and Supplementary Fig. 3e). Accordingly, mAbs against the major repeats of CSP from Pb, another rodent-infecting parasite (mAb 3D11), and from Pf, the most lethal human-infecting malaria parasite (mAb 2A10), are also cytotoxic to Pb and PfSPZs, respectively (Fig. 3h), showing that this unique killing activity of anti-repeats antibodies is species-transcendent.

Despite the killing activity of anti-repeats mAbs, ~20% of Pb and Py GFP-expressing SPZs, and ~50% of PfSPZs remain alive after incubation with high concentrations of cytotoxic mAbs. To determine if GFP expression could explain this difference, we compared the killing activity of J6 mAb on wild-type and GFP-expressing PySPZ. Since both parasites are equally susceptible to J6 cytotoxicity (Supplementary Fig. 3f), a potentiating effect of GFP expression in SPZ death was discarded. Interestingly, PbSPZs expressing a hybrid PbCSP harbouring the central part of the PfCSP[36] (Fig. 3h, PbPfSPZ) are as susceptible as PfSPZs to intermediate concentrations of the cytotoxic 2A10-anti-PfCSP repeats mAb. However, at high concentration, only ~20 and 50% of PbPfSPZs and PfSPZ remain alive, respectively (Fig. 3h). Since this percentage roughly corresponds to the population of immotile parasites in similar experimental conditions[37], we tested if the antibody cytotoxicity is dependent on SPZ motility.

As shown in the figure 4a, inhibition of actin polymerization by cytochalasin D (CD) at a concentration that blocks parasite motility[38], strongly reduces mAb cytotoxicity. After 45 minutes of incubation, however, a progressive killing is observed in the presence of CD (Fig. 4b, green squares), suggesting that a factor other than actin-dependent motility contributes to the parasite death. CSP is known to be secreted at the apical pole of SPZs and then translocated backwards, forming a thread-like precipitate at the posterior end of the SPZ in the presence of anti-repeats mAb[38] (circumsporozoite precipitation reaction, CSPR; Fig. 4c, J6 -CD). When CSP translocation is inhibited by CD, a vesicular and membranous extrusion is formed at the SPZ apical end[38] (Fig. 4c, J6 +CD). This turgid extrusion can be easily evidenced by microscopy and differentiated from the CSPR by the anterior staining of microtubules (Fig. 4c, tubulin). The absence of GFP signal in the CSPR and apical extrusion (AE) indicates that these structures are frequently devoid of cytoplasmic content. An exception is the punctual GFP fluorescence structure observed inside the CSPR (Fig. 4c, J6 -CD), similar to the persistent fluorescent signal observed during the dotty death. AE and CSPR are observed after SPZ incubation with W24 and J6, however, while the cytotoxic anti-repeats mAb mostly induces large, well-delineated and

refringent extensions at the anterior (strong AE) and posterior end of SPZs (strong CSPR), the anti-NT mAb induces amorphous and low-refringent structures (Fig. 4c, weak AE and CSPR). Both anti-CSP mAbs are thus capable of triggering an exacerbated secretion in PySPZs, albeit with different intensities (Fig. 4c). To determine if the strong oversecretion induced by J6 could be linked to PySPZ death, the intracellular calcium chelator BAPTA-AM, a known inhibitor of micronemal vesicular secretion[39] was tested in the presence of the cytotoxic mAb. Both strong AE (Fig. 4d) and J6 cytotoxicity (Fig. 4e) were inhibited by BAPTA-AM, indicating that micronemal secretion could be involved in the PySPZ killing. The fact that J6-treated PySPZs become permeable to PI through their anterior pole, the region of secretory granule discharge, added to the presence of a pore-forming like protein involved in the wounding of the host cell plasma membrane called SPECT2 (Sporozoite microneme Protein Essential for Cell Traversal 2, SP2)[6] in these granules, prompted us to test the role of SP2 in the SPZ killing by anti-repeats mAb. The disruption of the SP2 gene in PySPZs ($SP2^{ko}$)[40] rendered the knockout parasite resistant to J6-mediated killing despite the formation of the CSPR and the AE in CD-treated SPZs (Fig. 4f). Therefore, in the absence of SP2, the actin polymerization-dependent CSPR cannot lead alone to parasite death. Equally, apical oversecretion induced by J6 in CD-treated PySPZ SP2ko does not significantly affect parasite viability (Fig. 4f), showing that SP2 acts as a terminal effector in the J6-induced PySPZ death.

Since PySPZ death is associated with anterior secretion, actin polymerization and the presence of SP2, we hypothesize that CSP could be acting as a shield, inhibiting the insertion of this pore-forming like protein in the parasite membrane. Therefore, when the continuous anterior secretion and backwards shedding of CSP elicited by J6 deplete the secretory stock of CSP, the parasite membrane becomes devoid of this protective shield, starting at the anterior pole, and thus, susceptible to the SP2 cytotoxicity. Indeed, while almost all of J6-treated live GFP^{+} PySPZs display a $J6^{+}$ CSP staining shielding the entire SPZ body (Fig. 4g, PySPZ J6 live; $J6^{+}$: 32/34; ~94%), most of dead GFP^{-} PySPZs lack the CSP staining on the surface of their anterior end (Fig. 4g, PySPZ J6 dead; $J6^{-}$: 51/67; ~76%). Accordingly, the apical pole of $SP2^{ko}$ PySPZs is

predominantly J6^{-} following mAb-treatment, but PySPZs remain alive due to the absence of SP2 (Fig. 4g, PySP2ko J6 live; J6^{-}: 28/32; ~87%). Finally, the non-cytotoxic W24 mAb induces the shedding of the CSP population harbouring the NT region, but not of the processed CSP. This generates a body-labelling pattern positive for J6 and negative for W24 (Fig. 4g, PySPZ W24 live; J6^{+}W24^{-}: 39/43; ~91%), indicating that this J6^{+} CSP population is enough to protect W24-treated PySPZs from SP2 cytotoxicity.

PbSP2^{ko} SPZs are also much less susceptible to the killing activity of anti-repeats 3D11 cytotoxic antibody (Fig. 4h), despite having similar motile capacity in the absence or presence of mAb, as well as the same surface amount of CSP as control SPZs (Supplementary Fig. 4a-c). To distinguish a local and individual *cis*-effect of SP2 on SPZs from a *trans*-effect of SP2 released from antibody-killed parasites on the rest of SPZ population, we mixed PbRFP-expressing control parasites with PbGFP-expressing SP2^{ko} SPZs in the presence of different concentrations of cytotoxic antibody. Figure 4i shows that at killing concentrations of mAbs, the SP2 released from susceptible control SPZs does not increase the killing of PbGFP-SP2^{ko} SPZs, indicating that SP2 released from dying/dead parasites does not kill in *trans*. PbGFP and PbRFP control SPZs are equally susceptible to the cytotoxic mAb (Supplementary Fig. 4d).

In addition to SP2, the disruption of two other proteins, SPECT (SP)[41] and CelTOS[42], severely impairs the host-cell wounding capacity of PbSPZs (Fig. 4j). However, only the knockout of the SPZ-specific proteins, SP and SP2, decrease the cytotoxic activity induced by anti-repeats mAb (Fig. 4k). CelTOS is thought to target and wound the inner leaflet of the host cell plasma membrane[43], and accordingly, its disruption does not alter the antibody cytotoxicity.

Altogether these results indicate that CSP has a protective role, shielding the parasite against membrane-targeted cytotoxic proteins. Anti-CSP repeats mAbs trigger the oversecretion of apical vesicles containing CSP[44,45] and the cell wounding proteins, SP[41] and SP2[6]. Concomitantly, CSP is translocated and shed at the posterior pole of SPZs until stripped from the parasite surface. The exposition of the parasite membrane then renders SPZ susceptible to these secreted

cell-wounding proteins, which are final effectors of mAb-induced cytotoxic death (Supplementary Fig. 5).

By dissecting the determinants of protection associated with anti-PyCSP humoral immunity, we identify the skin as a critical site for protection and the mechanisms by which anti-CSP antibodies eliminate SPZs, via a singular cytotoxic activity. Our results support the notion that protective anti-CSP repeats antibodies preferentially target PySPZs in the cutaneous tissue[7,25], the physiological site of parasite inoculation. PySPZ neutralization in the blood is thus less efficient than in the skin[25]. Accordingly, sterile protection of passively immunized hosts against iv inoculation with SPZs is only effective at high concentrations of transferred mAbs[5,21,25] and/or using a small effective inoculum of infectious SPZs[21,22,25,46]. This lower neutralizing efficacy could explain the lack of protection of immunized hosts possessing high titers of anti-CSP antibodies when iv challenged with SPZs[26-28]. Remarkably, anti-repeats mAbs directly kill malaria SPZs in a species-transcendent manner, clarifying why pre-incubation with anti-repeats mAbs efficiently neutralizes SPZ infectivity[1-3]. In contrast to other anti-plasmodial cytotoxic antibodies[47,48], complement and FcRγ are not required as downstream host effectors. Cytotoxicity is instead dependent on intrinsic SPZ factors, such as parasite motility or proteins involved in the membrane wounding and traversal of host cells. Since these two factors are both indispensable for the parasite progression and exit from the dermis[7-9], cytotoxic concentrations of mAbs optimally target moving SPZs in the host skin. Strategies to improve the generation of potent immobilizing and cytotoxic antibodies might help to ameliorate the efficacy of CSP-based vaccines.

(2795 words)

Acknowledgements

We would like to thank the team of the Centre of Production and Infection of Anopheles, Institut Pasteur, in particular Marek Szatanik, Catherine Thouvenot, Sylvain Golba, Jennifer Pham, and Audrey Lorthiois for providing mosquitoes and *P. falciparum* SPZs; the team of the Platform of Dynamic Imaging, Institut Pasteur, in particular Dr Spencer Shorte and Marie-Anne Nicola for the access to the confocal microscopes and IVIS system; Dr Kami Kim from the Albert Einstein College of Medicine for providing the *P. yoelii* YM GFP-LUC; Dr Victor Nussenzweig from the New York University for providing the PbPf parasites; Dr Miguel Soares from the Instituto Gulbenkian for providing $J_HT^{-/-}$ mice; Dr Pierre-Marie Lledo and Dr Pierre Bruhns from the Institut Pasteur for providing, respectively, the C3$^{-/-}$ and the FcRgamma$^{-/-}$ mice; the team of the Clinical Investigation and Access to Bio Resources, in particular Marie-Noelle Ungeheuer for providing the red blood cells for the *P. falciparum* culture; Dr Patricia Baldacci and Dr Pauline Formaglio for their critical reading of the manuscript.

This work was supported by funds from the Institut Pasteur – Paris, the French National Research Agency (grant no. ANR-14-CE16-Im3alaria), the French Government's Investissement d'Avenir program, Laboratoire d'Excellence "Integrative Biology of Emerging Infectious Diseases" (grant no. ANR-10-LABX-62-IBEID) and "ParaFrap" (grant no. ANR-11-LABX-0024), the Sao Paulo Research Foundation (FAPESP – grant no. 2014/50631-0), the National Council for Scientific and Technological Development (CNPq), the BNP Paribas CIB, the Portuguese Science and Technology Foundation (FCT- IF/00881/2012/CP0158) and the European Social Fund (Human Potential Operating Programme).

R.A., S.B.B., E.A., J.T., conceived and designed the experiments. E.A., J.T., S.T., R.H.P, performed the experiments. M.M.Y., S.D. and F.T. generated the hybridomas. O.S., T.I. and M.Y. contributed with transgenic parasites. R.A., S.B.B, E.A., J.T., S.T., R.H.P., analysed the data. R.A, E.A, J.T. and S.B.B., wrote the paper.

Material and Methods

Parasites, mice and mosquitoes

We used *Plasmodium yoelii* 17XNL[49]; *Plasmodium yoelii* 17XNL expressing GFP under the control of the *pbef1αa* promoter[50] or hsp70 promoter[51]; *P. yoelii* 17XNL SPECT2^{ko} (PyΔ*plp1*) expressing GFP under the control of hsp70 promoter[40], *Plasmodium yoelii* YM expressing a GFP-luciferase (GFP-LUC) fusion protein under the control of elongation factor1α promoter[52]; *P. berghei* ANKA expressing GFP under the control of hsp70 promoter[53]; *P. berghei* cell traversal deficient parasites SPECT^{ko}, SPECT2^{ko}[9], and CelTOS^{ko} [42] expressing GFP under the control of hsp70 promoter, *P. berghei* ANKA expressing RFP under the control of *eef1-α*[54] promoter; *P. berghei* NK65 expressing GFP under the control of hsp70 promoter[55] and a hybrid CSP containing the tandem repeated region of *P. falciparum* CSP (PbPf-GPF) generated by crossing *P. berghei* NK65 expressing GFP with the parasite bearing the hybrid CSP[36], and *P. falciparum* NF54 [56].

BALB/cJRj, RjOrl:SWISS and C57BL/6JRj mice were purchased from Elevage Janvier. C57BL/6 $J_HT^{-/-}$ [57] mice were obtained from Instituto Gulbenkian de Ciência, kindly provided by Dr Miguel Soares. C3 ko mice B6.129S4-*C3*^{tm1Crr}/J[58] were kindly provided by Dr Pierre-Marie Lledo, and C57BL/6J-FcRg ko Fcer1g^{tm1Rav} [59] by Dr. Pierre Bruhns, both from the Institut Pasteur. All animal experiments were approved by the Animal Care and Use committee of Institut Pasteur (CETEA Institut Pasteur 2013-0093, Ministère de l'Enseignement Supérieur e de la Recherche MESR 01324) and were performed in accordance with European guidelines and regulations (directive 2010/63/EU). For all tests, 4-8 weeks old females were used, and allocate in cages randomly. Immunization experiments were performed using five to ten animals per experiment, which gives a significance threshold of 75 to 50% of sterile protection using Fisher's Exact Test. SPZ challenge was blind, but not immunization.

Anopheles stephensi mosquitoes (Sda500 strain) were reared in the Centre for Production and Infection of Anopheles (CEPIA) at the Institut Pasteur using standard procedures. For the production of rodent *Plasmodium spp.* SPZs, mosquitoes were fed on infected RjOrl:SWISS mice 1–2 d after emergence and kept in a humidified chamber at 24°C (Py) or 21°C (Pb). One week after infection, Py infected mosquitoes were fed on naïve RjOrl:SWISS mice. Infected mosquitoes used for natural transmission experiments (15-18 days after the infectious blood meal) were deprived of sucrose for one day before experimentation to enhance the rate of mosquito bites. For intravenous and footpad injections Py SPZs were collected from infected salivary glands 15–22 d after the infectious blood meal. Pb SPZs were collected from infected salivary glands 21-28 d after the infectious blood meal.

For the production of *P. falciparum* SPZs, gametocytes were cultivated in human Rh+ erythrocytes (ICAReB, Institut Pasteur) at 7% haematocrit in RPMI 1640 medium, 25 mM HEPES, 0.37 mM hypoxanthine, 10% AB+ human serum (Etablissement Français du Sang), at 37° C, 5% CO_2, 1% O_2, 94% N_2. After 14 days in an automated culture system [60], mature gametocytes were checked by microscopy with Giemsa staining on blood smears and tested for exflagellation. Female *Anopheles gambiae* or *stephensi* mosquitoes were fed on a membrane feeder with gametocytes resuspended in human serum AB+ and fresh Rh+ erythrocytes (v/v) 2-4 days after emergence. Mosquitoes were kept at 26°C, 70% humidity and on 10% sucrose. Seven days after the infective blood meal, mosquitoes were fed on non-infected Rh+ RBCs and AB+human serum. Salivary glands SPZs were collected in phosphate buffered saline at days 17-21.

Recombinant PyCSP and peptides.

The PyCSP open reading frame without the signal peptide and GPI anchor signal sequence (accession number P06914; amino acids 23 to 346) was codon optimized and cloned in a bacterial expression vector pET21b to produce a recombinant protein with 6x histidine residues at the C terminal end. The recombinant protein was produced in *E. coli* BL21 Star (DE3)

(Invitrogen) upon induction with 1mM IPTG. Purification was accomplished using Ni-NTA super flow resin under native conditions, according to the manufacturer's instructions. The several fractions containing the purified protein were joined and subjected to a PD-10 desalting column (GE Healthcare) and the imidazole was removed by the gravitational method (as per manufacturer's instructions) using PBS. Endotoxins were removed using two-phase extraction with Triton-X114[61] and their residual levels were determined using the Pierce *Limulus* amebocyte lysate (LAL) chromogenic quantitation assay (TermoFisher Scientific). All protein batches used for immunization had final endotoxin levels bellow 1 EU/mL. After removal of endotoxins, protein concentration was determined by semi-quantitative SDS-PAGE stained with Coomassie Blue using BSA as a standard. The N-Terminal (amino acids 23 to 138) and the C-Terminal (amino acids 260 to 346) regions of PyCSP were cloned and expressed as described above to determine by ELISA the specificity of the mAbs generated. Sequence of peptides used to determine anti-PyCSP repeats mAbs: QGPGAPQGPGAPQGPGAP and QQPPQQPPQQPP.

Mice immunizations and sera/mAb transfer

BALB/cJRj, C57BL/6JRj,, C57BL/6 $J_HT^{-/-}$ mice were immunized with 5-15 μg of PyCSP and 50 μg Poly (I:C) HMW (InvivoGen, USA) as adjuvant (A) in PBS containing 1% Glycerol (Sigma) and 50mM Imidazole (Sigma). Naive mice or mice immunized with the adjuvant alone served as controls. The formulation was administered intraperitoneally (ip) in a total volume of 100 μL. Animals were primed, and boosted two weeks later. Passive sera transfer was performed by iv administration of 0.5 mL of serum collected from individual mice 2 weeks after immunization (as described above). MAbs were injected ip (100-150 μg/mouse) diluted in PBS, 24 hours before the SPZ challenge[62].

SPZ Challenge

Py SPZs collected from the salivary glands of infected *A. stephensi* mosquitoes were inoculated iv in the tail vein using a 30-Gx1/2" needle in a U-100 insulin syringe, or in the footpad skin using

35- to 36-G needle with a NanoFil syringe (World Precision Instruments) in naïve, control or immunized mice. Unless stated otherwise, 5,000 SPZs were microinjected in the skin. Mice challenge experiments by mosquito bites were done using *A. stephensi* mosquitoes infected with *P. yoelii* 17XNL GFP. Mice anesthetized with a mixture of ketamine (50 mg/kg body weight, Imalgene 1000, Merial) and xylazine (5 mg/kg body weight, 2% Rompun, Bayer) were bitten by 4 to 7 infected mosquitoes during 10-15 minutes. Challenges were performed two weeks after immunization boost, or the following day after sera/mAb transfer. Parasite load in the liver (using *P. yoelii YM* GFP-LUC) was assessed at 46 hours after infection by measuring whole mice bioluminescence upon injection of 150 mg/kg luciferin potassium salt (Perkin Elmer) and using an IVIS LUMINA II (Perkin Elmer). Parasitemia was determined by thin blood smears or flow cytometry, performed 3-12 days after SPZ challenge. Quantitative analysis of protection was determined using the log of the parasitemia at day 4 post-infection when the blood parasites are still growing exponentially. Sterile protection was defined as the absence of blood stage parasites after day 10 post-challenge. At least 20 microscopic fields (10,000–15,000 red blood cells) or 200,000 red blood cells were examined by flow cytometry for each mouse designated as protected.

Cells depletion

The antibodies were purchased from BioXcell, unless otherwise indicated. CD4 or CD8 T cells depletion was performed according to Schmidt et al. [63]. Briefly, immunized mice received ip a dose of 400 µg of rat IgG, anti-CD4 (clone GK1.5), or anti-CD8 (clone 2.43) antibodies on day −3 and day −1 prior to challenge with SPZs. Cell depletion in the blood was confirmed prior to challenge by analyzing $CD4^+$ (clone RM4-5, BioLegend) and $CD8^+$ (clone 53-6.7) T cell populations (gated on $CD3^+$, BioLegend). $Ly6G^+$ cells depletion was performed according to Jaeger, et al. [64]. Each mouse received a dose of 100 µg of rat IgG2b (clone LFT-2), 100 µg of rat anti-Gr-1 (clone RB6-8C5), or 500 µg of rat anti-Ly6G (clone 1A8) on days -5 and -3 prior to

challenge with SPZ. Depletion was verified by analysing CD11b$^+$ (clone M1/70, BDBiosciences) and Ly6C$^+$ cells (clone AL-21, BDBiosciences).

SPZ Imaging in the skin

Intravital imaging was performed using high-speed spinning disk confocal microscopy [65]. Briefly, Py GFP SPZs were microinjected in the previously epilated ear pinnae of anaesthetized control or immunized BALB/cJRj mice using a microsyringe (NanoFil 10 µL syringe, World Precision Instruments). When indicated, blood vessels were previously labelled by the iv injection of 50 µg of Alexa Fluor™ 647 BSA (Molecular Probes™). The mouse was positioned with the ear flattened on a slide. Images were acquired in different focal planes and analysed using the software ImageJ. The speed of SPZs was calculated for one minute of analysis during the first five minutes post-injection

In vitro gliding assay

The gliding assay was performed using 18 well µ-slide ibiTreat. All materials were kept on ice. Each test was performed individually. Each well contained 20 µL of a suspension in PBS with 5,000 GFP SPZ, 10% FCS, and different concentrations of mAbs when indicated. The slide was centrifuged for 3 min at 500 rcf, 4° C, and transferred to the microscope chamber, which was kept at 37°C, and 5% CO_2. After 5 min of incubation, images were acquired every second, during 2 minutes in an inverted AxioObserver microscope (Zeiss). Two-minutes maximal projections of SPZ trajectories were analysed and circular gliding, defined as a circular motion of crescent-shaped SPZ, was quantified using the software ImageJ. The speed of SPZs was determined using the plugin MTrackJ from ImageJ. Briefly, the images acquired were loaded on ImageJ, and manual tracking of moving SPZs was performed. The average speed was calculated considering the length travelled and the time of acquisition. For the *in vitro* analysis, only SPZs that moved in circular motion during the entire acquisition period were considered.

MAb library

MAbs were produced by the hybridoma technology based on the protocol of Köhler and Mielstein[66]. Mice were immunized using the recombinant PyCSP and the immunization protocol described above. Two weeks after the administration of the booster dose, splenocytes were fused with P3U1 (ECACC 85011417) or with P3x63Ag8.653 (ATCC Number CRL-1580™) myeloma cells. Other mAbs were produced by hybridoma cell lines already established, such as 3D11 anti-Pb CSP repeats (MRA-100, BEI Resources)[67], and 2A10, anti-Pf CSP repeats (MRA-183, BEI Resources)[68]. These cells were not tested for mycoplasma contamination. MAbs were purified from culture supernatants by affinity chromatography using protein G beads (GE healthcare). ELISA using the supernatant was performed for identification of wells containing anti-PyCSP antibody secreting cells. Wells were coated overnight at 4° C with recombinant PyCSP, or its fractions for the specificity determination. After blocking, supernatants or purified antibodies were incubated for 2 hours at 37°C, washed and detected using anti-mouse IgG coupled with peroxidase for 1 hour at 37°C followed by development with TMB. For isotyping, wells were coated with rabbit anti-mouse IgG (H+L) antibody, and detection was done using antibodies anti-IgG and light chain isotypes coupled to peroxidase. The epitope sequences recognized by two anti-NT mAbs were identified using an array containing linear 15-mer peptides with 14-mer peptide-peptide overlap of the entire PyCSP ORF (Pepperprint). The detection was done using Cy3 goat anti-mouse IgG (H+L), and the array was scanned on a motorized stage of an inverted microscope.

In vitro SPZ killing test – viability assay

Unless otherwise stated, GFP SPZs from salivary glands were incubated at 37°C for 45 min, except when otherwise indicated, with 10% FCS in PBS in the presence of different mAbs concentrations. When indicated, 0.5 μM cytochalasin D (Sigma) and/or 100 μM BAPTA-AM (Sigma) was added. J6 mAb was heat inactivated (h.i.) at 70° C for 20 min. After incubation, parasites were kept on ice and incubated with 5 μg/mL propidium iodide (Invitrogen). Viability

was determined by flow cytometry as the percentage of $GFP^{+}PI^{-}$ SPZs to the sum of $GFP^{+}PI^{-}$ and $GFP^{-}PI^{+}$ SPZs. The gating strategy is described in the legend of the Supplementary Figure 3. In the case of non-fluorescent Py or Pf SPZ, they were identified using 0.5 µg/mL of Alexa Fluor™ 647 conjugated J6, or 2A10, respectively. For Pb and Pf SPZ, the mAbs W24 and E12 were used as isotype controls, respectively. At least 1,500 events in the SPZ gate were acquired on CytoFLEX S flow cytometer (Beckman Coulter), and analysed using the softwares CytExpert 2.0 (Beckman Coulter) or FlowJo 10.2 (FlowJo LLC).

SPZ immunostaining

For the surface CSP staining, 50,000 GFP SPZs from salivary glands were incubated on ice with 5 µg/mL of different mAbs in PBS for 60 minutes. For CSP quantification in Pb or PySPZ surface, 0.1 or 1 µg/mL of mAb was used. After washing, SPZs were incubated on ice with 4 µg/mL Alexa Fluor™ 647 conjugated anti-mouse IgG (H+L) (Invitrogen) in PBS, and analysed by flow cytometry. The Alexa Fluor™ 647 median of fluorescence was determined from the GFP-positive population in a SSC-H vs GFP-H pseudocolor plot (at least 1,000 events). Data were acquired on a FACSCalibur (Becton Dickinson) or CytoFLEX S flow cytometer (Beckman Coulter), and analysed on the software CytExpert 2.0 (Beckman Coulter) or FlowJo 10.2 (FlowJo LLC). For the secretion analysis, after incubation with 100 µg/mL of mAbs ± 0.5-1 µM CD as described for the viability assay, PyGFP SPZ were fixed in 2% PFA, permeabilized with 0.3% Triton X-100, and stained with 0.25 µg/mL of anti-α-Tubulin (11H10) Alexa Fluor™ 647 (Cell Signaling Technology), 2 µg/mL of goat anti-mouse IgG (H+L) Alexa Fluor™ 350, and 2 µg/mL of Hoechst 33342. When indicated, W24-treated PyGFP SPZ were incubated with J6 conjugated with Alexa Fluor™ 647. Images were acquired using an inverted AxioObserver microscope (Zeiss).

Host cell wounding assay

The assay was performed based on Prudêncio et al. [69]. Briefly, HepG2 cells obtained from the American Type Culture Collection (ATCC Number HB-8065™) were maintained in high glucose

Dulbecco's Modified Eagle Medium GlutaMAX™ (Gibco) containing 10% FCS (Biowest) and 1% MEM Non-essential Amino Acids solution (100X) (Sigma-Aldrich) on flasks coated with collagen. They were not authenticated in our lab, nor tested for mycoplasma contamination. Cells were trypsinized and seeded on 96-well plates 24 hours before infection (50,000 cells/well coated with collagen). Pb GFP control and cell wounding deficient mutant SPZs (12,500 SPZ; MOI 1:4) in the presence of 1 mg/mL Tetramethylrhodamine Dextran (DxRed), lysine fixable, 10,000 MW (Molecular Probes) were transferred to wells with HepG2 cells. The plate was centrifuged for 5 min at 500 rcf, and incubated for 2 hours at 37 °C, 5% CO_2 and 10% O_2. Cytochalasin D (Sigma) at the concentration of 0.5 μM was used as negative control for cell wounding. The HepG2 population (10,000 events acquired) was identified on a FSC-A vs SSC-A pseudocolor plot, followed by singlet isolation in a FSC-A vs FSC-H plot. GFP positive events were considered as invaded cells, and DxRed positive as wounded cells (Supplementary figure 4e). The gating population of the latter was determined by mechanically wounding cells using a pipette tip, and comparing it to the control. Data were acquired on a CytoFLEX S flow cytometer (Beckman Coulter), and analysed using the softwares CytExpert 2.0 (Beckman Coulter) or FlowJo 10.2 (FlowJo LLC).

Statistical analysis

Statistical significances were determined by one-way ANOVA with Holm-Sidak correction for multiple comparisons, two-tailed Fisher's Exact Test, or two-tailed unpaired t test. Analyses were calculated using GraphPad Prism version 6 for Mac OS X.

Data availability

The data that support the findings of this study are available from the corresponding author upon request.

Figure Legends

Figure 1: Sterilizing anti-PyCSP humoral immunity is dependent on the host skin inoculation with SPZs. (a) Schematic representation of Py17X CSP (P06914.1) and the recombinant protein used in this study ($PyCSP_{23-346}$). Signal peptide (SP), N-Terminal (NT), C-Terminal (CT) and the GPI-anchor signal sequence (GPIa). Sequences of major (QGPGAP) and minor (QQPP) PyCSP repeats. (b) Immunization and challenge schedule using the recombinant PyCSP and PySPZs. (c) Parasite load in the liver determined by bioluminescence imaging. Adjuvant (A) or adjuvant + PyCSP (A.CSP) immunized BALB/cJRj mice. Bars represent the average ± SD of the log of average radiance in the liver measured in photons/sec/cm^2/sr (n=5 mice, circles) from one out of three independent experiments. Dotted line indicates the background level (bk) of bioluminescence in non-infected tissue. Representative images of the parasite bioluminescence show the liver infection. Heat map of radiance in photons/sec/cm^2/sr. (d, e) Percentage of blood infected mice immunized with A or A.CSP after challenge. (d) PySPZs inoculated in the mouse footpad (skin), by mosquito bite, or iv, (n=8 BALB/cJRj mice). Pooled data from two independent experiments are shown. (e) PyGFP:LUC SPZs microinjected in the mouse footpad of control C57BL/6JRj or $J_HT^{-/-}$. Pooled data from two independent experiments. (c-e) On the top of the panels, numbers of blood infected mice at day 10 post-challenge out of total challenged mice. Significance determined by two-tailed unpaired t test (c) or two-tailed Fisher's Exact Test (d, e).

Figure 2. Decrease of motility and killing of parasites in the skin of CSP-immunized mice. (a) Motility of PyGFP SPZs observed in the skin of mice immunized with the adjuvant (A) or the adjuvant + PyCSP (A.CSP). Images represent maximal projections of the SPZ trajectories (red) during 60 seconds. The initial position of each parasite is represented in yellow. Representative result of three independent experiments. Scale bars, 20 μm. (b) Relative SPZ velocity normalized by the average speed of adjuvant control. Graph shows average ± SD of n=82 PySPZ for A, n=61 PySPZ for A.CSP from three independent experiments. (c) Time-lapse of SPZs in the skin of A.CSP immunized mice exemplifying the dotty death phenotype. Left panel shows the fluorescent dot (arrowhead) formed in the posterior region of a SPZ, and the loss of its fluorescence following the waning of the SPZ body fluorescence. Right panel shows the apparent detachment of a fluorescent and stable dot structure (arrowhead) from the SPZ body. Note that a second evanescent dot (arrowhead) appears during the SPZ death. (d) Quantification of dotty death phenotype as represented in (c). Left: time-lapse sequence of SPZs inoculated in the skin of mice immunized with A (red) or A.CSP (green). Right: bars represent the average ± SD of the percentage of dotty death phenotype (arrowheads) during the first 30 min of recording from at least three independent experiments. (e) Time-lapse sequence showing, in the upper panel, the dotty death (arrowhead) of a SPZ in the skin of a mouse immunized with A.CSP. In the lower panel (intravasation, red arrowhead, narrowing of SPZ body), a SPZ is shown invading an Alexa Fluor™ 647-BSA labeled blood vessel (white). In the third image, the projection of frames spanning one minute shows the SPZ being carried away with the blood flow. (c-e) Time is indicated in white at the corner of the pictures. Scale bars, 10 μm. (c, e) SPZs are pseudo-colored based on their depth, indicated by the color code on the right. Asterisks indicate the anterior pole of SPZs. (b, d) Statistical significance determined by two-tailed unpaired t test.

Figure 3. Complement and FcRγ-independent cytotoxic antibody sterilizes SPZ infection. (a) Protection after anti-PyCSP mAbs passive transfer (n=4 BALB/cJRj mice from one experiment). (b) Protection of passively immunized mice following PySPZ inoculation by different routes (n=8 BALB/cJRj mice from two independent experiments). (c) Protection of C57BL/6 C3 knockout mice (n=6 mice for group W24 C57BL/6 $C3^{-/-}$, and n=7 for the others, from two independent experiments), or (d) C57BL/6 FcRgamma knockout mice (n=7 mice from one experiment) passively immunized with mAbs. (a, c, d) PySPZs were microinjected in the skin. (a-d) Graphs represent log of parasitemia ± SD at day four after challenge. N.I., not infected. All N.I. mice from the J6 group at day 4 were sterile protected with a single exception in the group C57BL/6 $FcRg^{-/-}$. (e) Normalized *in vitro* gliding velocity of PySPZ in the presence of mAbs. Graph shows individual values (symbols) and average (lines) ± SD (n=15 PySPZs per concentration). Representative result of two independent experiments. On the right, 12-second pseudo-colored projections using 25 (J6) or 100 (W24) μg/mL. (f) Time-lapse sequence showing the killing activity of J6 on live PySPZs. Time is indicated on the upper right corner. Asterisk indicates SPZ anterior end. Representative result of two independent experiments. (e, f) Scale bar, 10 μm. (g) Viability curve of PySPZs incubated with different mAbs. Result of at least three independent experiments. On the top, scheme of the PyCSP regions recognized by each mAb and sequences of the major (QGPGAP) and minor (QQPP) repeats. On the right, live PySPZ surface recognition by the anti-CSP mAbs. Histogram shows representative binding profiles (red) compared to control without primary antibody (blue). (h) Viability of Pf, PbPf, and Pb SPZs after incubation with anti-CSP repeats mAbs: 2A10 for PfCSP repeats, and 3D11 for PbCSP repeats (n=3 independent experiments). On the top, scheme of CSPs from each species, and amino acid sequences of each repeat region. (g, h) Graphs show average ± SD. (a-e) Statistical significance determined by one-way ANOVA with Holm-Sidak correction for multiple comparisons.

Figure 4. Motility, secretion and SPZ-specific wounding proteins play a critical role in the death mediated by the cytotoxic antibody. (a) Viability of SPZs incubated with 50 µg/mL mAbs±CD (n=2 for Py W24, and n=3 independent experiments for other groups) (b) Kinetics of PySPZ death mediated by mAbs±CD. Graph represents viability of one out of two independent experiments. (c) IFA of PySPZ treated with mAb±CD. Pie charts: quantification of color-coded characteristics (weak (red)/strong (blue) circumsporozoite precipitation reaction (CSPR) and weak (orange)/strong (grey) apical extrusion (AE)). Representative images of merged fluorescence (left), and bright-field (BF, right pictures) of PySPZs. (d) Inhibition of AE by BAPTA-AM in J6±CD-treated PySPZs. Graph shows percentage of SPZ displaying the characteristics represented on the right, as described in (c). Numbers of quantified SPZs on the top of bars. Results from two independent experiments. Asterisk indicates apical, and arrowhead, posterior pole. (e) Viability of mAbs±BAPTA-AM-treated PySZP (n=2 independent experiments). (f) Viability of mAbs±CD-treated control and SP2^{ko} PySPZ (n=3 independent experiments). Right: representative images from one out of two independent experiments of J6±CD-treated Py SP2^{ko} SPZ, and quantification of SPZs as described in (c). (g) Representative images of mAbs-treated PySPZ (n=3 independent experiments for PySPZ and n=1 for PySP2^{ko} SPZ). Images show merged (first column) and individual markers (subsequent columns). Pie charts on the right display the quantification of apical labeled (J6^{+}/J6^{+}W24^{-}) and unlabeled (J6^{-}) PySPZ. (h) Viability of control and SP2^{ko} PbSPZ treated with mAbs (n=3 independent experiments). (i) Left: percentage of live PbRFP^{+} control and PbGFP^{+} SP2^{ko} SPZ after incubation with 3D11. Representative result of two independent experiments. Right: pseudocolor-plots of the live SPZ populations (colored arrowheads). In the upper right corner, 3D11 concentration (µg/mL). (j) Wounded HepG2 cells by control or cell wounding deficient PbSPZ mutants. Graph shows percentage of wounded cells (n=1 experiment in triplicate). (k) Viability of control and cell wounding-deficient PbSPZ treated with 3D11. Result from one out of two independent experiments. (a, e, f, h, k) Graphs show average ± SD. (c, d, f, g) Scale bar: 10 µm. Statistical significance determined by one-way ANOVA with Holm-Sidak correction for multiple comparisons (a, f,) or two-tailed Fisher's exact test (d).

Supplementary figure 1: Protection of immunized mice depends on SPZ inoculation into the skin. (a) Comparison of parasite load in the liver of naïve BALB/cJRj mice 46 hours after infection with 5,000, 2,500 or 1,250 PySPZs by iv injection (red circles) compared to 5,000 SPZs by microinjection in the mouse footpad (skin, black circles) (n=3 mice). Graph show average ± SD of the log of average radiance in the liver measured in photons/sec/cm^2/sr. (b) Parasite load in the liver of mice immunized with A.CSP or only with A, and challenged with either 5,000 or 2,500 PyGFP:LUC SPZs, by the iv (n=4 mice) or skin (n=6 mice) route of inoculation. On the top, representative images of the parasite bioluminescence show liver infection. Data show individual values (symbols) and the average (bars) ± SD of the log of average radiance in the liver measured in photons/sec/cm^2/sr. (a, b) Dotted line indicates the background level (bk) of bioluminescence in non-infected tissue. (c) Comparison of parasitemia in naïve BALB/cJRj mice after iv injection (red circles) or microinjection in the mouse footpad (skin, black circles) of 250 (iv only), 500 (skin only), 1,250, 2,500, or 5,000 PySPZs. Graph represents the average ± SD of the log of parasitemia on day 3 after SPZ inoculation of one experiment (n= 7 mice). Statistical significance determined by two-sided unpaired t test (b).

Supplementary figure 2: Protection of mice challenged with SPZs is mediated by humoral immunity. (a) Detection of T cells ($CD3^+$) subsets in the peripheral blood of control or $CD4^+$/$CD8^+$ depleted BALB/cJRj mice immunized with A or A.CSP. Graph shows individual values (symbols), and average (bars) ± SD from one experiment (n=4 mice for control IgG and anti-CD4, and n=5 mice for anti-CD8 group). (b) Parasite load in the liver of mice immunized with A or A.CSP and T cell depleted (anti-CD4 or anti-CD8) or not (Control IgG). Data show individual values (symbols) and average (bars) ± SD of the log of average radiance in the liver measured in photons/sec/cm^2/sr from one experiment (n=4 mice for control IgG, n=5 for anti-CD8, and n=3 for anti-CD4 group). (c) Detection of neutrophils ($Ly6C^{INT}$, $CD11b^+$, black bars) and inflammatory monocytes ($Ly6C^{HI}$ $CD11b^+$, white bars) in the peripheral blood of BALB/cJRj mice immunized with A or A.CSP after injection of control IgG (LFT2 clone), anti-neutrophil/ inflammatory

monocytes (RB6-8C5 clone), and anti-neutrophil (1A8 clone) mAbs. Data show individual values (symbols) and average (bars) ± SD of log of percentage of cells from one experiment (n=6 mice). (d) Log of parasitemia of individual mice immunized with A (circles), or A.CSP (triangles) in neutrophil/ inflammatory monocytes depleted mice, neutrophil depleted mice or control mice 4 days after the challenge. Graph shows individual values (symbols) and average (bars) ± SD of groups of one experiment (n=6 mice). N.I., not infected. (e) Parasite load in the liver of BALB/cJRj mice after passive transference of sera from immunized mice. Data show the average ± SD of the log of average radiance in the liver from one experiment (n=4 mice). On the top, representative images of liver infection by bioluminescent parasites. Heat map of radiance and bars expressed in photons/sec/cm^2/sr. (b, e) Dotted line indicates the background level (bk) of bioluminescence in non-infected tissue. Statistical significance was determined by one-way ANOVA with Holm-Sidak correction for multiple comparisons (a-d) or two-sided unpaired t test (e).

Supplementary figure 3: *In vivo* protection of mice passively immunized with mAbs depends on the inoculation site of SPZs, cytotoxic assay by flow cytometry and *in vivo* protection of mAb 15D7. (a) Parasitemia curve of BALB/cJRj mice challenged by iv inoculation with 250 PySPZs (left panel) or by footpad (skin) inoculation with 500 PySPZs (right panel). Graphs show the log of percentage of parasitemia of individual mice transferred or not with 150 µg of J6 mAb one day before challenge. Result from one experiment (n= 7 mice). Lines correspond to the linear regression and 95% confidence interval. (b) Parasitemia on the fourth day after PySPZ inoculation of the groups described in (a). Graph shows individual values (symbols) and average (bars) ± SD of the log of parasitemia (n=7 mice). (c, d) Example of pseudocolor plots of the viability assay after SPZ incubation with no antibody or with cytotoxic mAb for 45 minutes at 37 °C. Representative result of at least twenty independent experiments. (c) Gating of the SPZ population. The SPZ population was independently validated based on the GFP fluorescence or surface CSP staining using an Alexa Fluor™ 647-labeled anti-CSP antibody.

The GFP^{-}PI^{+} population was determined using a cytotoxic antibody. (d) SPZ viability assay based on the uptake of propidium iodide (PI, red) and loss of SPZ GFP fluorescence (green) in the SPZ population gated in (c). (e) Parasitemia curve of BALB/cJRj mice challenged with 5,000 PySPZs one day after ip injection of 100 µg of mAb (15D7 or control mAb) or PBS. Result expressed as log of percentage of parasitemia of individual mice and curve as average of distribution from one experiment (n=4 mice). (f) Viability of non-fluorescent (PyWT, red symbols), and GFP-expressing (PyGFP, green symbols) SPZ treated with different concentrations of J6 (circles), and 100 µg/mL of W24 (triangles). Values represent percentage of viable SPZs from one experiment in duplicate. Statistical significance determined by two-sided unpaired t test (b). (a,b,e) N.I.,not infected. All N.I. mice at day 4 post-challenge were sterile protected.

Supplementary figure 4: Motility, surface CSP and cytotoxicity controls, and gating strategy for the cell wounding assay.

(a) Comparison between control (Con) and SP2^{ko} PbSPZs regarding their capacity to perform circular gliding *in vitro.* Graph shows individual values (symbols) and average (bars) ± SD percentage of the total population (n=3 independent experiments). (b) Comparison of the gliding velocity in the presence or absence of cytotoxic mAb. Relative SPZ velocity normalized by the average speed of the control (Pbcon without mAb) is shown. Graph represents values of individual SPZs (symbols) and average (red line) ± SD. Numbers of analyzed SPZ are shown on the top of the graph. Result from two independent experiments. (c) Determination of surface CSP staining by flow cytometry using mAb 3D11 and a fluorescent secondary antibody. On the left, histograms of the fluorescence intensity. On the right, graph showing relative surface CSP staining normalized by the median fluorescence intensity (FI) of the control (blue). Individual values (symbols) and average (bars) ± SD are represented. 2^{ary}, secondary antibody only (n=3 independent experiments). (d) Percentage of live PbRFP^{+} control (red) and PbGFP^{+} control (green) after incubation with 3D11 mAb (one out of two independent experiments). Right panels show pseudocolor-plots of the respective live SPZ populations (colored arrowheads). The

concentration of 3D11 mAb (μg/mL) is represented in the upper right corner. Statistical significance was determined by two-sided unpaired t test (a, c), or one-way ANOVA with Holm-Sidak correction for multiple comparisons (b). (e) Gating strategy for the host-cell wounding assay. The first pseudocolor plot shows the region of interest for the detection of HepG2 cells, followed by the identification of the singlet population and the quantification of wounded cells (DxRed positive cells in the two upper quadrants).

Supplementary figure 5: Model of SPZ killing by anti-CSP repeats antibodies

(a) Anti-repeats cytotoxic J6 mAb induces an intracellular calcium-dependent oversecretion, leading to the actin polymerization-dependent CSPR. When the CSP (purple coat) is stripped from the SPZ surface, its plasma membrane becomes exposed and susceptible to the action of the secreted pore-forming like protein, SP2, which causes the parasite death. (b) Anti-NT non-cytotoxic W24 mAb induces an intracellular calcium-dependent oversecretion, leading to the actin polymerization-dependent CSPR. When the non-processed CSP (orange coat) is stripped from the SPZ surface, the processed CSP (blue coat), lacking the NT region, still shields the SPZ plasma membrane rendering the parasite resistant to the cytotoxic effect of SP2. (c) J6 induces intracellular calcium-dependent oversecretion, leading to the actin polymerization-dependent CSPR. When the CSP is completely stripped from the surface of the SP2 knockout SPZ, the parasite does not die, despite having the plasma membrane exposed, due to the lack of the pore-forming like protein, SP2.

Supplementary table 1. Characterization of the anti-CSP monoclonal antibodies.

For each anti-PyCSP mAb used in this work, the CSP region recognized by ELISA using the recombinant PyCSP $_{23\text{-}138}$ (NT region), the $(QGPGQP)_3$ peptide (Major repeats) or the $(QQPP)_3$ peptide(Minor repeats) is shown. The sequence of the linear epitope recognized using a 15-mer peptides with 14-mer peptide-peptide overlap covering the entire PyCSP is shown between <>. Information on the isotype, and constant light chains is also provided, as well as the binding

intensity to the CSP on the surface of SPZs by IFA/cytometry (Live SPZ) or to the recombinant PyCSP $_{23\text{-}346}$ by ELISA (ELISA rPyCSP).

References

1 Yoshida, N., Nussenzweig, R. S., Potocnjak, P., Nussenzweig, V. & Aikawa, M. Hybridoma produces protective antibodies directed against the sporozoite stage of malaria parasite. *Science* **207**, 71-73 (1980).

2 Nardin, E. H. *et al.* Circumsporozoite proteins of human malaria parasites Plasmodium falciparum and Plasmodium vivax. *J Exp Med* **156**, 20-30 (1982).

3 Cochrane, A. H., Santoro, F., Nussenzweig, V., Gwadz, R. W. & Nussenzweig, R. S. Monoclonal antibodies identify the protective antigens of sporozoites of Plasmodium knowlesi. *Proc Natl Acad Sci U S A* **79**, 5651-5655 (1982).

4 Charoenvit, Y. *et al.* Inability of malaria vaccine to induce antibodies to a protective epitope within its sequence. *Science* **251**, 668-671 (1991).

5 Charoenvit, Y. *et al.* Monoclonal, but not polyclonal, antibodies protect against Plasmodium yoelii sporozoites. *J Immunol* **146**, 1020-1025 (1991).

6 Ishino, T., Chinzei, Y. & Yuda, M. A Plasmodium sporozoite protein with a membrane attack complex domain is required for breaching the liver sinusoidal cell layer prior to hepatocyte infection. *Cell Microbiol* **7**, 199-208, doi:CMI447 [pii]10.1111/j.1462-5822.2004.00447.x (2005).

7 Vanderberg, J. P. & Frevert, U. Intravital microscopy demonstrating antibody-mediated immobilisation of Plasmodium berghei sporozoites injected into skin by mosquitoes. *Int J Parasitol* **34**, 991-996, doi:10.1016/j.ijpara.2004.05.005S0020751904001171 [pii] (2004).

8 Amino, R. *et al.* Quantitative imaging of Plasmodium transmission from mosquito to mammal. *Nat Med* **12**, 220-224, doi:nm1350 [pii]10.1038/nm1350 (2006).

9 Amino, R. *et al.* Host cell traversal is important for progression of the malaria parasite through the dermis to the liver. *Cell Host Microbe* **3**, 88-96, doi:S1931-3128(08)00002-4 [pii]10.1016/j.chom.2007.12.007 (2008).

10 Menard, R. *et al.* Circumsporozoite protein is required for development of malaria sporozoites in mosquitoes. *Nature* **385**, 336-340, doi:10.1038/385336a0 (1997).

11 Pancake, S. J., Holt, G. D., Mellouk, S. & Hoffman, S. L. Malaria sporozoites and circumsporozoite proteins bind specifically to sulfated glycoconjugates. *J Cell Biol* **117**, 1351-1357 (1992).

12 Sidjanski, S. P., Vanderberg, J. P. & Sinnis, P. Anopheles stephensi salivary glands bear receptors for region I of the circumsporozoite protein of Plasmodium falciparum. *Mol Biochem Parasitol* **90**, 33-41, doi:S0166-6851(97)00124-2 [pii] (1997).

13 Cerami, C. *et al.* The basolateral domain of the hepatocyte plasma membrane bears receptors for the circumsporozoite protein of Plasmodium falciparum sporozoites. *Cell* **70**, 1021-1033, doi:0092-8674(92)90251-7 [pii] (1992).

14 Tewari, R., Spaccapelo, R., Bistoni, F., Holder, A. A. & Crisanti, A. Function of region I and II adhesive motifs of Plasmodium falciparum circumsporozoite protein in sporozoite motility and infectivity. *J Biol Chem* **277**, 47613-47618, doi:10.1074/jbc.M208453200 (2002).

15 Gilson, P. R. *et al.* Identification and stoichiometry of glycosylphosphatidylinositol-anchored membrane proteins of the human malaria parasite Plasmodium falciparum. *Mol Cell Proteomics* **5**, 1286-1299, doi:10.1074/mcp.M600035-MCP200 (2006).

16 Olotu, A. *et al.* Seven-Year Efficacy of RTS,S/AS01 Malaria Vaccine among Young African Children. *N Engl J Med* **374**, 2519-2529, doi:10.1056/NEJMoa1515257 (2016).
17 White, M. T. *et al.* The relationship between RTS,S vaccine-induced antibodies, CD4(+) T cell responses and protection against Plasmodium falciparum infection. *PLoS One* **8**, e61395, doi:10.1371/journal.pone.0061395 (2013).
18 Stewart, M. J., Nawrot, R. J., Schulman, S. & Vanderberg, J. P. Plasmodium berghei sporozoite invasion is blocked in vitro by sporozoite-immobilizing antibodies. *Infect Immun* **51**, 859-864 (1986).
19 Hollingdale, M. R., Zavala, F., Nussenzweig, R. S. & Nussenzweig, V. Antibodies to the protective antigen of Plasmodium berghei sporozoites prevent entry into cultured cells. *J Immunol* **128**, 1929-1930 (1982).
20 Hollingdale, M. R., Nardin, E. H., Tharavanij, S., Schwartz, A. L. & Nussenzweig, R. S. Inhibition of entry of Plasmodium falciparum and P. vivax sporozoites into cultured cells; an in vitro assay of protective antibodies. *J Immunol* **132**, 909-913 (1984).
21 Potocnjak, P., Yoshida, N., Nussenzweig, R. S. & Nussenzweig, V. Monovalent fragments (Fab) of monoclonal antibodies to a sporozoite surface antigen (Pb44) protect mice against malarial infection. *J Exp Med* **151**, 1504-1513 (1980).
22 Egan, J. E. *et al.* Efficacy of murine malaria sporozoite vaccines: implications for human vaccine development. *Science* **236**, 453-456 (1987).
23 Tan, J. *et al.* A public antibody lineage that potently inhibits malaria infection through dual binding to the circumsporozoite protein. *Nat Med* **24**, 401-407, doi:10.1038/nm.4513 (2018).
24 Kisalu, N. K. *et al.* A human monoclonal antibody prevents malaria infection by targeting a new site of vulnerability on the parasite. *Nat Med* **24**, 408-416, doi:10.1038/nm.4512 (2018).
25 Sack, B. K. *et al.* Model for in vivo assessment of humoral protection against malaria sporozoite challenge by passive transfer of monoclonal antibodies and immune serum. *Infect Immun* **82**, 808-817, doi:10.1128/IAI.01249-13 (2014).
26 Sedegah, M. *et al.* Evaluation of vaccines designed to induce protective cellular immunity against the Plasmodium yoelii circumsporozoite protein: vaccinia, pseudorabies, and Salmonella transformed with circumsporozoite gene. *Bull World Health Organ* **68 Suppl**, 109-114 (1990).
27 Collins, W. E. *et al.* Immunization of Saimiri sciureus boliviensis with recombinant vaccines based on the circumsporozoite protein of Plasmodium vivax. *Am J Trop Med Hyg* **40**, 455-464 (1989).
28 Lal, A. A. *et al.* In vivo testing of subunit vaccines against malaria sporozoites using a rodent system. *Proc Natl Acad Sci U S A* **84**, 8647-8651 (1987).
29 Belmonte, M. *et al.* The infectivity of Plasmodium yoelii in different strains of mice. *J Parasitol* **89**, 602-603, doi:10.1645/0022-3395(2003)089[0602:TIOPYI]2.0.CO;2 (2003).
30 Gueirard, P. *et al.* Development of the malaria parasite in the skin of the mammalian host. *Proc Natl Acad Sci U S A* **107**, 18640-18645, doi:10.1073/pnas.1009346107 (2010).
31 Bongfen, S. E. *et al.* The N-terminal domain of Plasmodium falciparum circumsporozoite protein represents a target of protective immunity. *Vaccine* **27**, 328-335, doi:10.1016/j.vaccine.2008.09.097 (2009).

32 Herrera, R. *et al.* Reversible Conformational Change in the Plasmodium falciparum Circumsporozoite Protein Masks Its Adhesion Domains. *Infect Immun* **83**, 3771-3780, doi:10.1128/IAI.02676-14 (2015).
33 Espinosa, D. A. *et al.* Proteolytic Cleavage of the Plasmodium falciparum Circumsporozoite Protein Is a Target of Protective Antibodies. *J Infect Dis* **212**, 1111-1119, doi:10.1093/infdis/jiv154 (2015).
34 Noris, M. & Remuzzi, G. Overview of complement activation and regulation. *Semin Nephrol* **33**, 479-492, doi:10.1016/j.semnephrol.2013.08.001 (2013).
35 Nimmerjahn, F. & Ravetch, J. V. Fcgamma receptors: old friends and new family members. *Immunity* **24**, 19-28, doi:10.1016/j.immuni.2005.11.010 (2006).
36 Persson, C. *et al.* Cutting edge: a new tool to evaluate human pre-erythrocytic malaria vaccines: rodent parasites bearing a hybrid Plasmodium falciparum circumsporozoite protein. *J Immunol* **169**, 6681-6685 (2002).
37 Vanderberg, J. P. Studies on the motility of Plasmodium sporozoites. *J Protozool* **21**, 527-537 (1974).
38 Stewart, M. J. & Vanderberg, J. P. Malaria sporozoites release circumsporozoite protein from their apical end and translocate it along their surface. *J Protozool* **38**, 411-421 (1991).
39 Carey, A. F. *et al.* Calcium dynamics of Plasmodium berghei sporozoite motility. *Cell Microbiol* **16**, 768-783, doi:10.1111/cmi.12289 (2014).
40 Risco-Castillo, V. *et al.* Malaria Sporozoites Traverse Host Cells within Transient Vacuoles. *Cell Host Microbe* **18**, 593-603, doi:10.1016/j.chom.2015.10.006 (2015).
41 Ishino, T., Yano, K., Chinzei, Y. & Yuda, M. Cell-passage activity is required for the malarial parasite to cross the liver sinusoidal cell layer. *PLoS Biol* **2**, E4, doi:10.1371/journal.pbio.0020004 (2004).
42 Kariu, T., Ishino, T., Yano, K., Chinzei, Y. & Yuda, M. CelTOS, a novel malarial protein that mediates transmission to mosquito and vertebrate hosts. *Mol Microbiol* **59**, 1369-1379, doi:MMI5024 [pii]10.1111/j.1365-2958.2005.05024.x (2006).
43 Jimah, J. R. *et al.* Malaria parasite CelTOS targets the inner leaflet of cell membranes for pore-dependent disruption. *Elife* **5**, doi:10.7554/eLife.20621 (2016).
44 Fine, E., Aikawa, M., Cochrane, A. H. & Nussenzweig, R. S. Immuno-electron microscopic observations on Plasmodium knowlesi sporozoites: localization of protective antigen and its precursors. *Am J Trop Med Hyg* **33**, 220-226 (1984).
45 Posthuma, G. *et al.* Immunogold determination of Plasmodium falciparum circumsporozoite protein in Anopheles stephensi salivary gland cells. *Eur J Cell Biol* **49**, 66-72 (1989).
46 Wang, R. *et al.* Induction of protective polyclonal antibodies by immunization with a Plasmodium yoelii circumsporozoite protein multiple antigen peptide vaccine. *J Immunol* **154**, 2784-2793 (1995).
47 Yilmaz, B. *et al.* Gut microbiota elicits a protective immune response against malaria transmission. *Cell* **159**, 1277-1289, doi:10.1016/j.cell.2014.10.053 (2014).
48 Bouharoun-Tayoun, H., Oeuvray, C., Lunel, F. & Druilhe, P. Mechanisms underlying the monocyte-mediated antibody-dependent killing of Plasmodium falciparum asexual blood stages. *J Exp Med* **182**, 409-418 (1995).

49 Weinbaum, F. I., Evans, C. B. & Tigelaar, R. E. An in vitro assay for T cell immunity to malaria in mice. *J Immunol* **116**, 1280-1283 (1976).
50 Ono, T., Tadakuma, T. & Rodriguez, A. Plasmodium yoelii yoelii 17XNL constitutively expressing GFP throughout the life cycle. *Exp Parasitol* **115**, 310-313, doi:10.1016/j.exppara.2006.09.008 (2007).
51 Manzoni, G. *et al.* A rapid and robust selection procedure for generating drug-selectable marker-free recombinant malaria parasites. *Sci Rep* **4**, 4760, doi:10.1038/srep04760 (2014).
52 Mwakingwe, A. *et al.* Noninvasive real-time monitoring of liver-stage development of bioluminescent Plasmodium parasites. *J Infect Dis* **200**, 1470-1478, doi:10.1086/606115 (2009).
53 Ishino, T., Orito, Y., Chinzei, Y. & Yuda, M. A calcium-dependent protein kinase regulates Plasmodium ookinete access to the midgut epithelial cell. *Mol Microbiol* **59**, 1175-1184, doi:MMI5014 [pii]10.1111/j.1365-2958.2005.05014.x (2006).
54 Sturm, A. *et al.* Alteration of the parasite plasma membrane and the parasitophorous vacuole membrane during exo-erythrocytic development of malaria parasites. *Protist* **160**, 51-63, doi:S1434-4610(08)00061-8 [pii]10.1016/j.protis.2008.08.002 (2009).
55 Demarta-Gatsi, C. *et al.* Immunological memory to blood-stage malaria infection is controlled by the histamine releasing factor (HRF) of the parasite. *Sci Rep* **7**, 9129, doi:10.1038/s41598-017-09684-2 (2017).
56 Ponnudurai, T., Leeuwenberg, A. D. & Meuwissen, J. H. Chloroquine sensitivity of isolates of Plasmodium falciparum adapted to in vitro culture. *Trop Geogr Med* **33**, 50-54 (1981).
57 Gu, H., Zou, Y. R. & Rajewsky, K. Independent control of immunoglobulin switch recombination at individual switch regions evidenced through Cre-loxP-mediated gene targeting. *Cell* **73**, 1155-1164 (1993).
58 Wessels, M. R. *et al.* Studies of group B streptococcal infection in mice deficient in complement component C3 or C4 demonstrate an essential role for complement in both innate and acquired immunity. *Proc Natl Acad Sci U S A* **92**, 11490-11494 (1995).
59 Takai, T., Li, M., Sylvestre, D., Clynes, R. & Ravetch, J. V. FcR gamma chain deletion results in pleiotrophic effector cell defects. *Cell* **76**, 519-529 (1994).
60 Ponnudurai, T., Lensen, A. H. & Meuwissen, J. H. An automated large-scale culture system of Plasmodium falciparum using tangential flow filtration for medium change. *Parasitology* **87 (Pt 3)**, 439-445 (1983).
61 Liu, S. *et al.* Removal of endotoxin from recombinant protein preparations. *Clin Biochem* **30**, 455-463 (1997).
62 Foquet, L. *et al.* Vaccine-induced monoclonal antibodies targeting circumsporozoite protein prevent Plasmodium falciparum infection. *J Clin Invest* **124**, 140-144, doi:10.1172/JCI70349 (2014).
63 Schmidt, N. W., Butler, N. S., Badovinac, V. P. & Harty, J. T. Extreme CD8 T cell requirements for anti-malarial liver-stage immunity following immunization with radiation attenuated sporozoites. *PLoS Pathog* **6**, e1000998, doi:10.1371/journal.ppat.1000998 (2010).
64 Jaeger, B. N. *et al.* Neutrophil depletion impairs natural killer cell maturation, function, and homeostasis. *J Exp Med* **209**, 565-580, doi:10.1084/jem.20111908 (2012).

65 Amino, R. *et al.* Imaging malaria sporozoites in the dermis of the mammalian host. *Nat Protoc* **2**, 1705-1712, doi:nprot.2007.120 [pii]10.1038/nprot.2007.120 (2007).
66 Kohler, G. & Milstein, C. Continuous cultures of fused cells secreting antibody of predefined specificity. *Nature* **256**, 495-497 (1975).
67 Eichinger, D. J., Arnot, D. E., Tam, J. P., Nussenzweig, V. & Enea, V. Circumsporozoite protein of Plasmodium berghei: gene cloning and identification of the immunodominant epitopes. *Mol Cell Biol* **6**, 3965-3972 (1986).
68 Zavala, F. *et al.* Rationale for development of a synthetic vaccine against Plasmodium falciparum malaria. *Science* **228**, 1436-1440 (1985).
69 Prudencio, M., Rodrigues, C. D., Ataide, R. & Mota, M. M. Dissecting in vitro host cell infection by Plasmodium sporozoites using flow cytometry. *Cell Microbiol* **10**, 218-224, doi:CMI1032 [pii]10.1111/j.1462-5822.2007.01032.x (2008).

Figure 1. Aliprandini et al

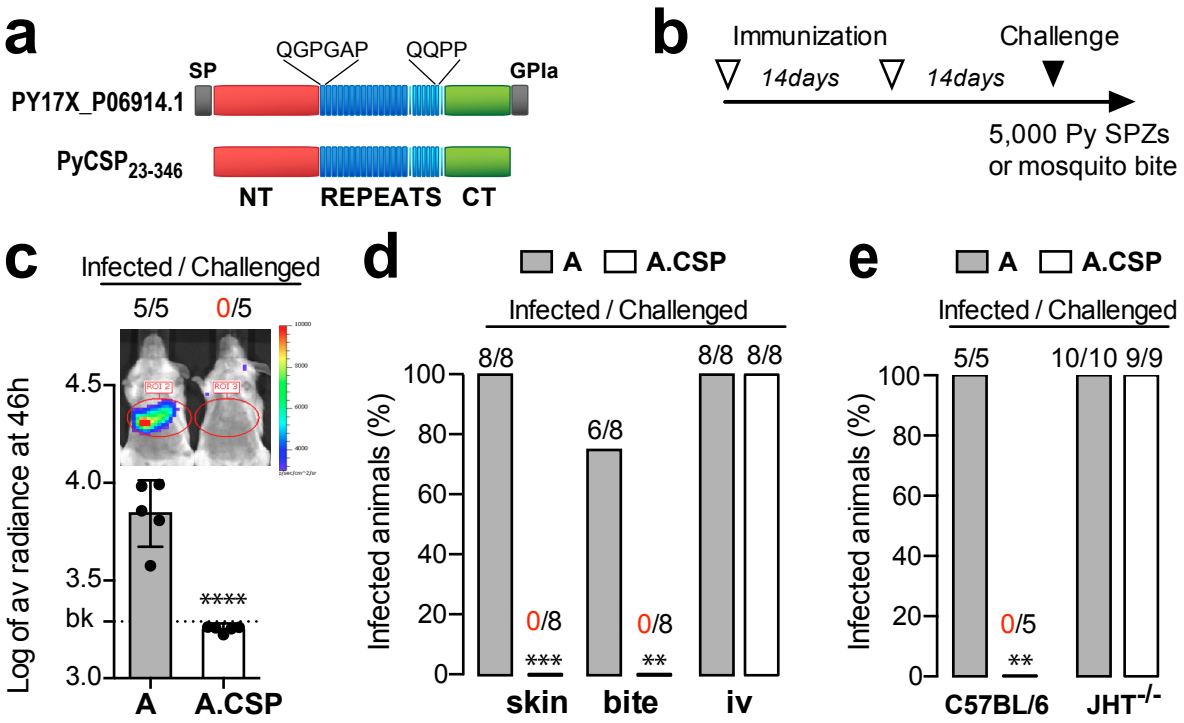

Figure 2. Aliprandini et al

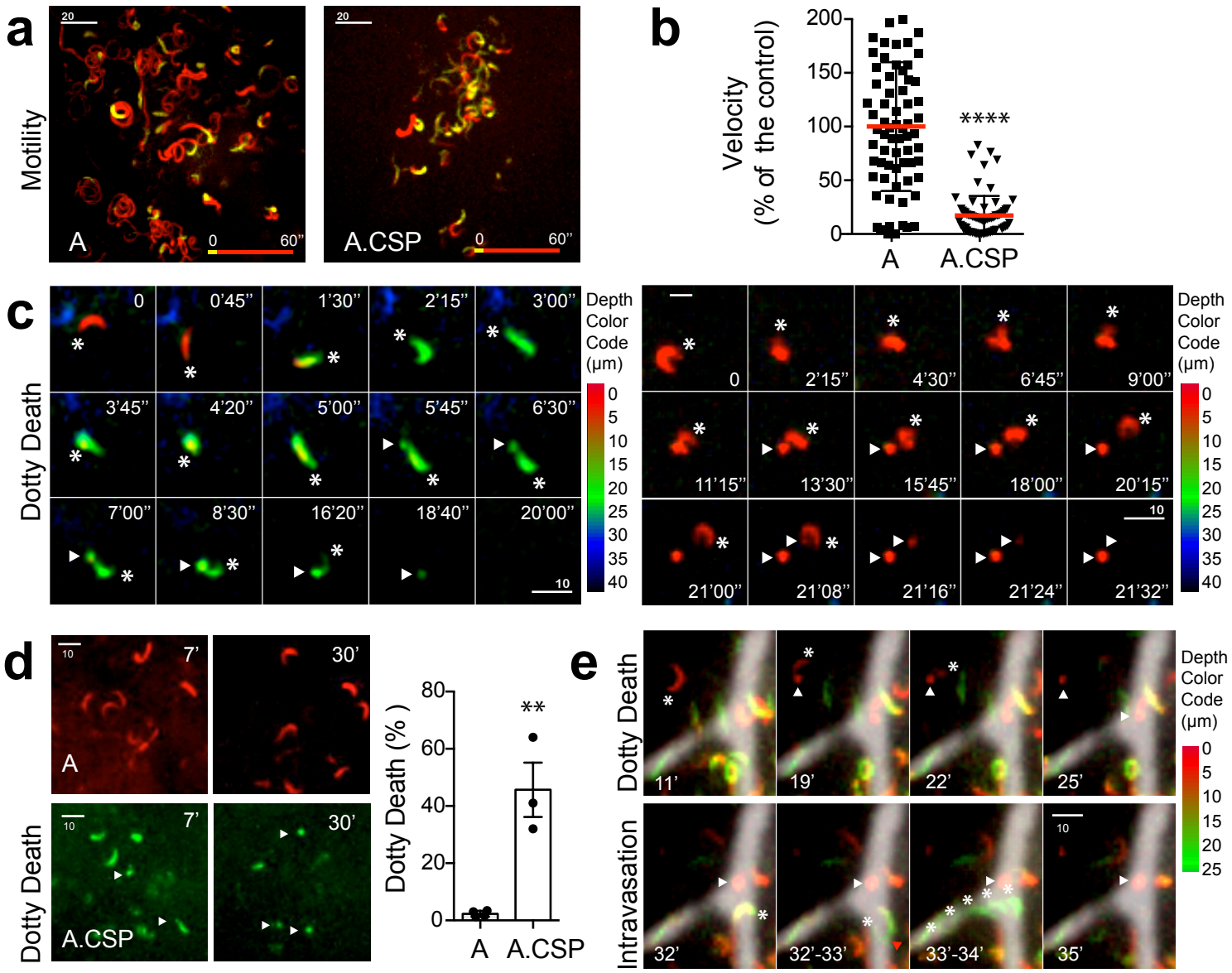

Figure 3. Aliprandini et al

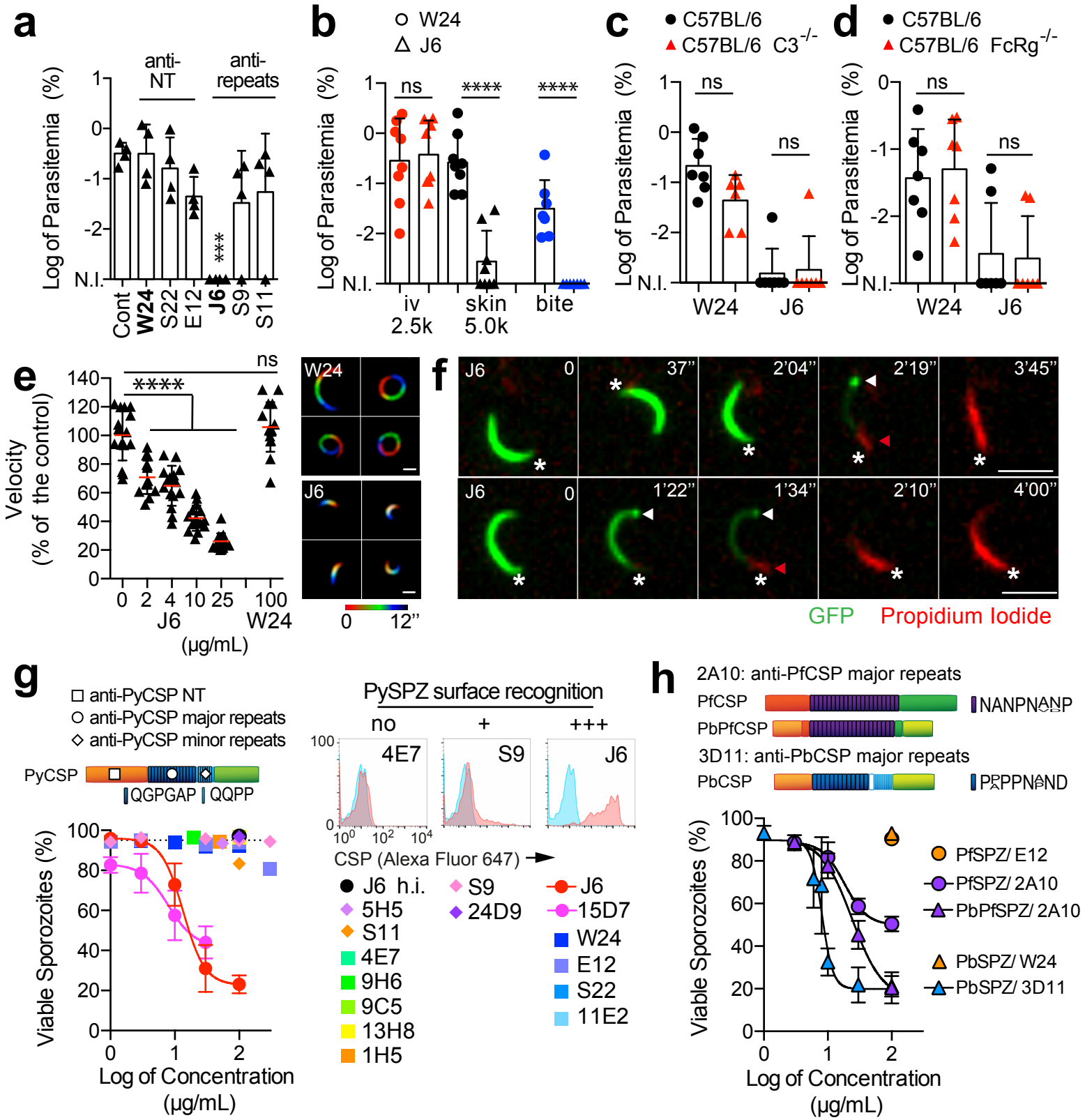

Figure 4. Aliprandini et al

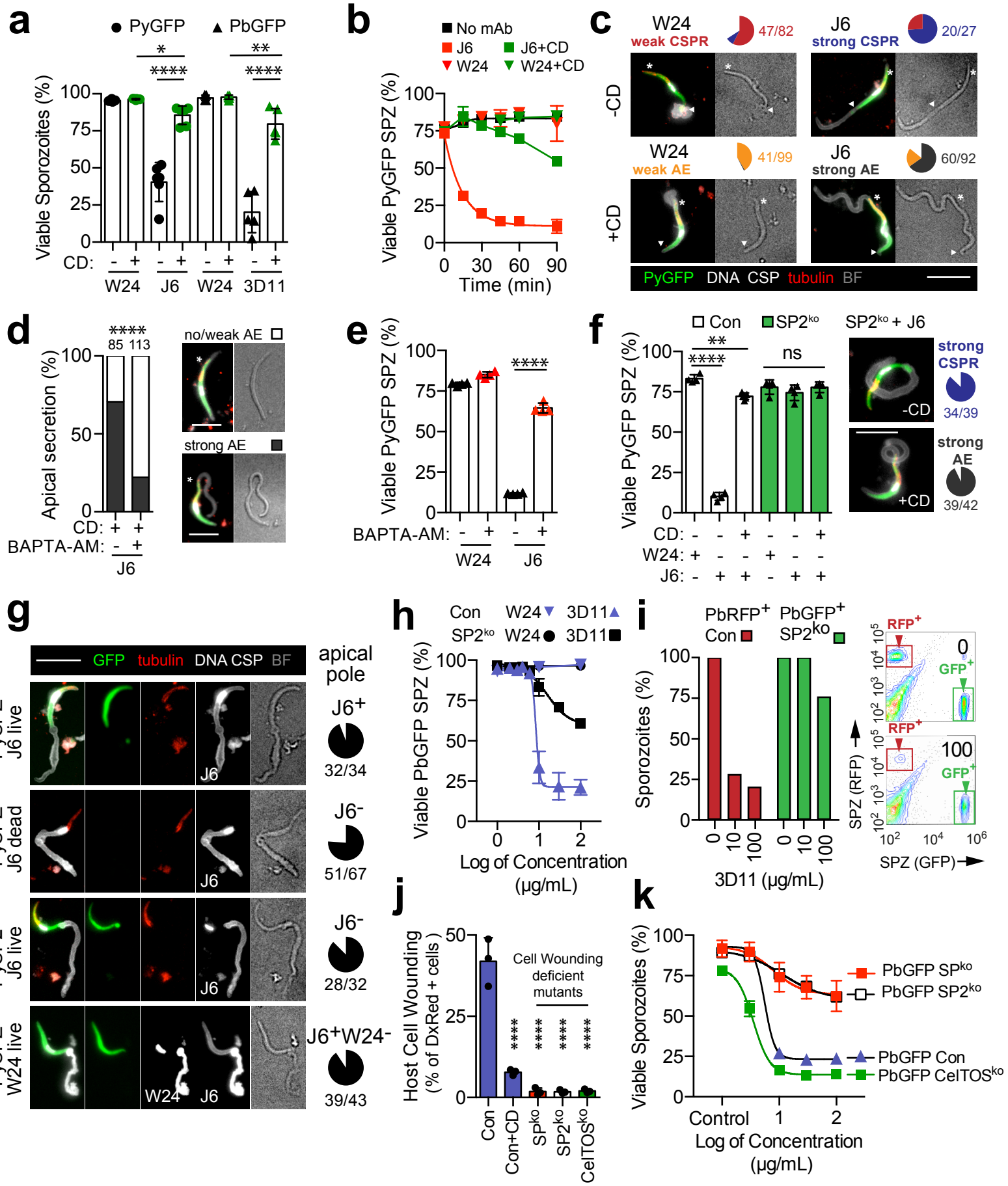

Figure S1. Aliprandini et al

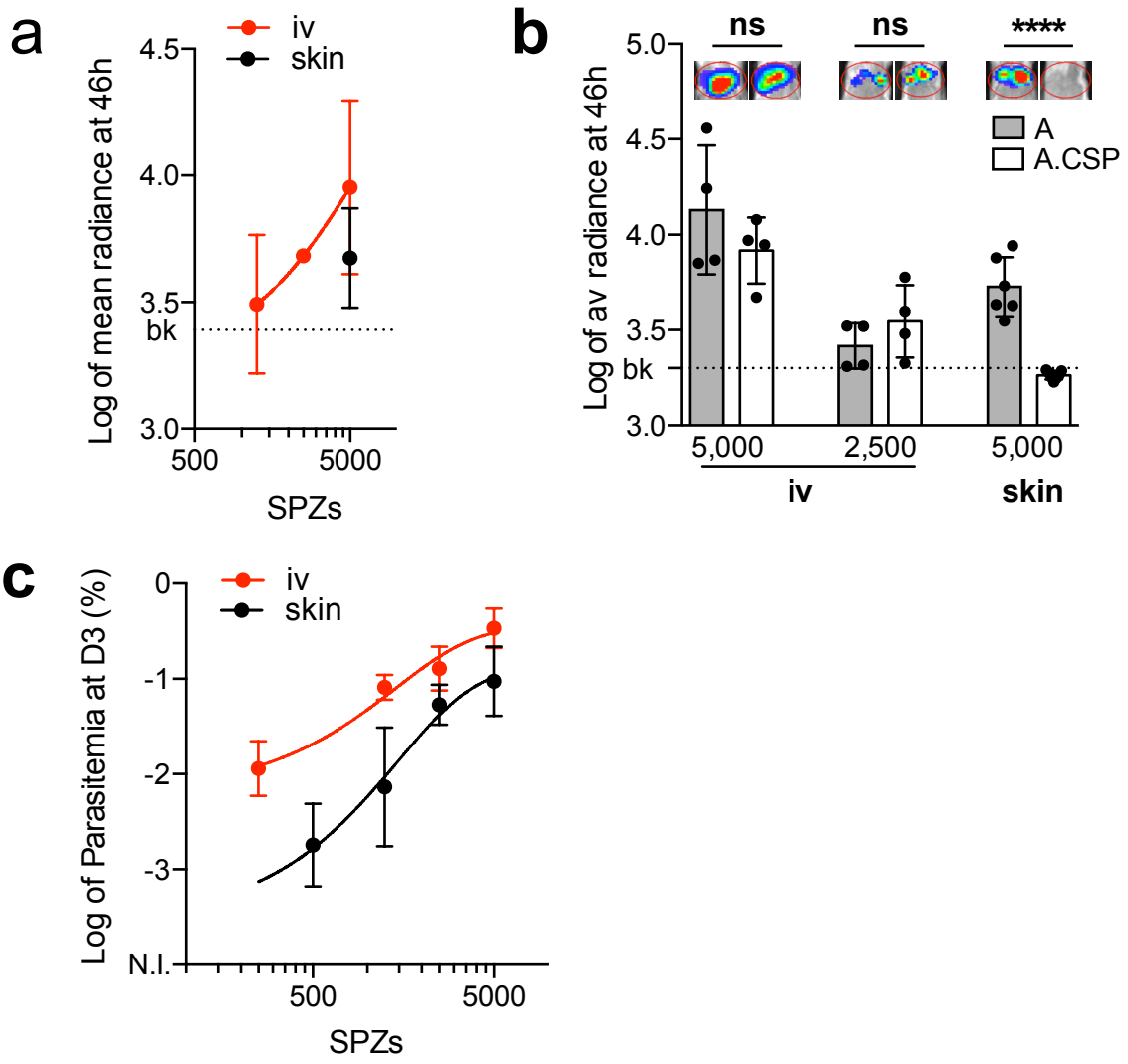

Figure S2. Aliprandini et al

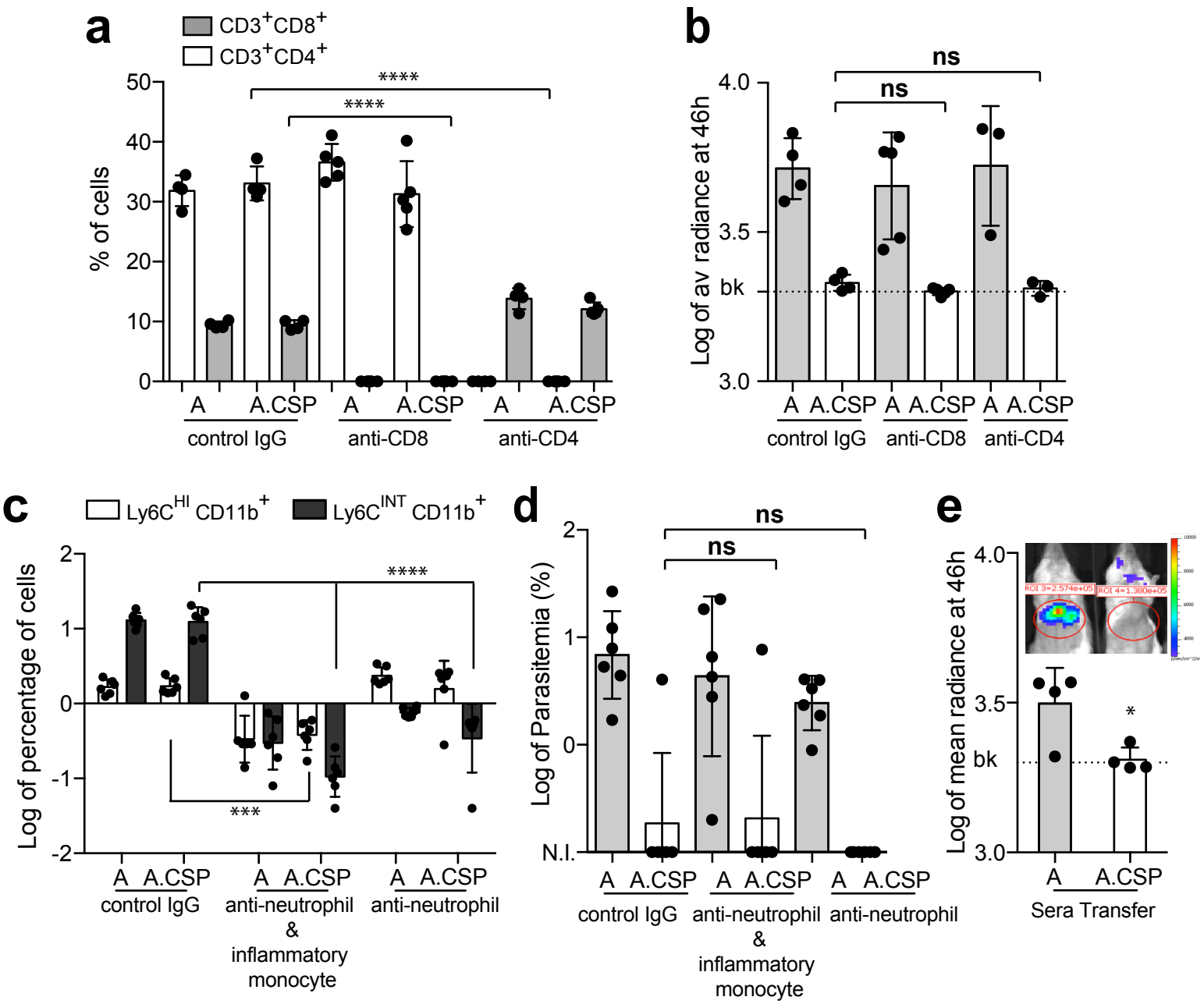

Figure S3. Aliprandini et al

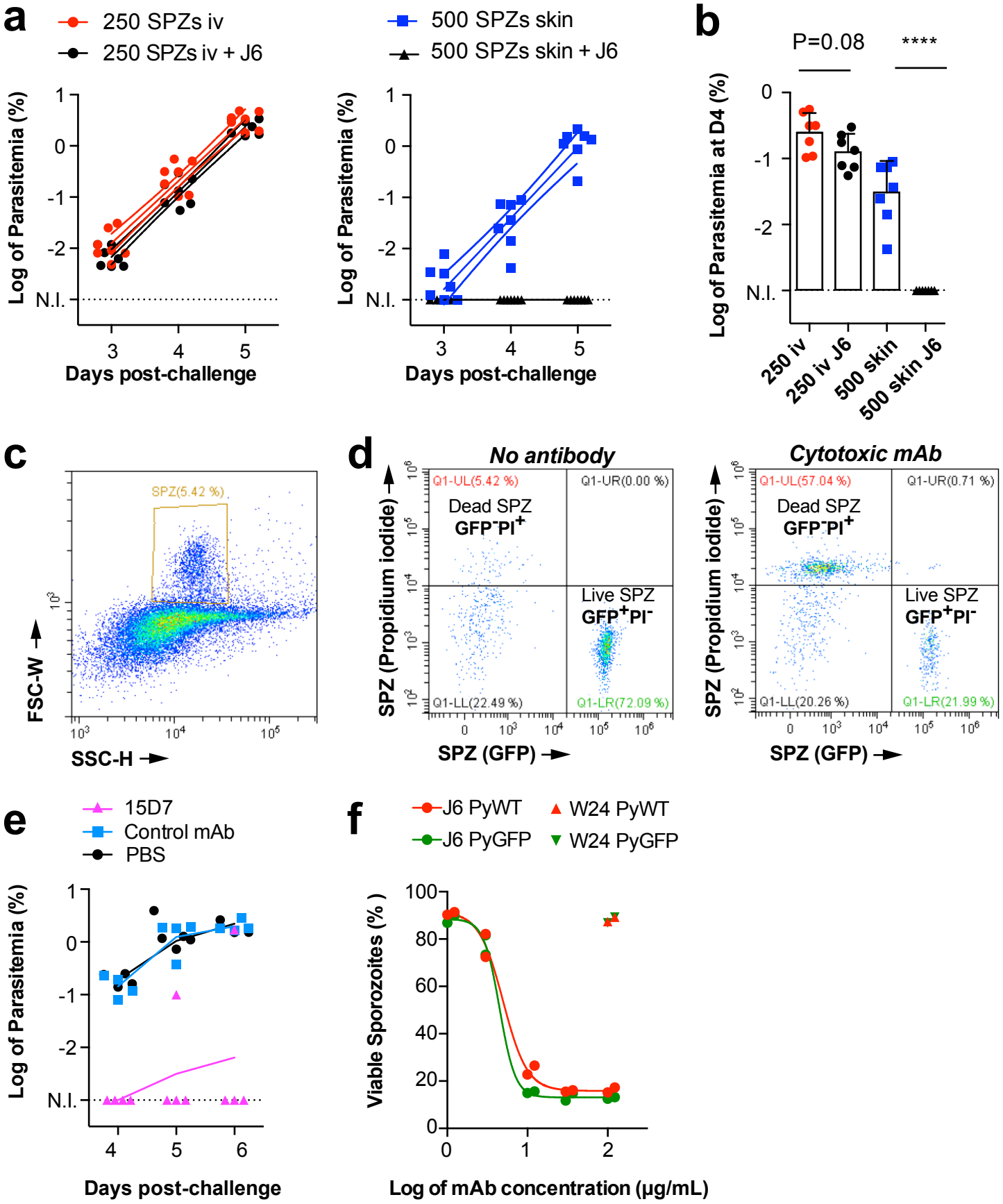
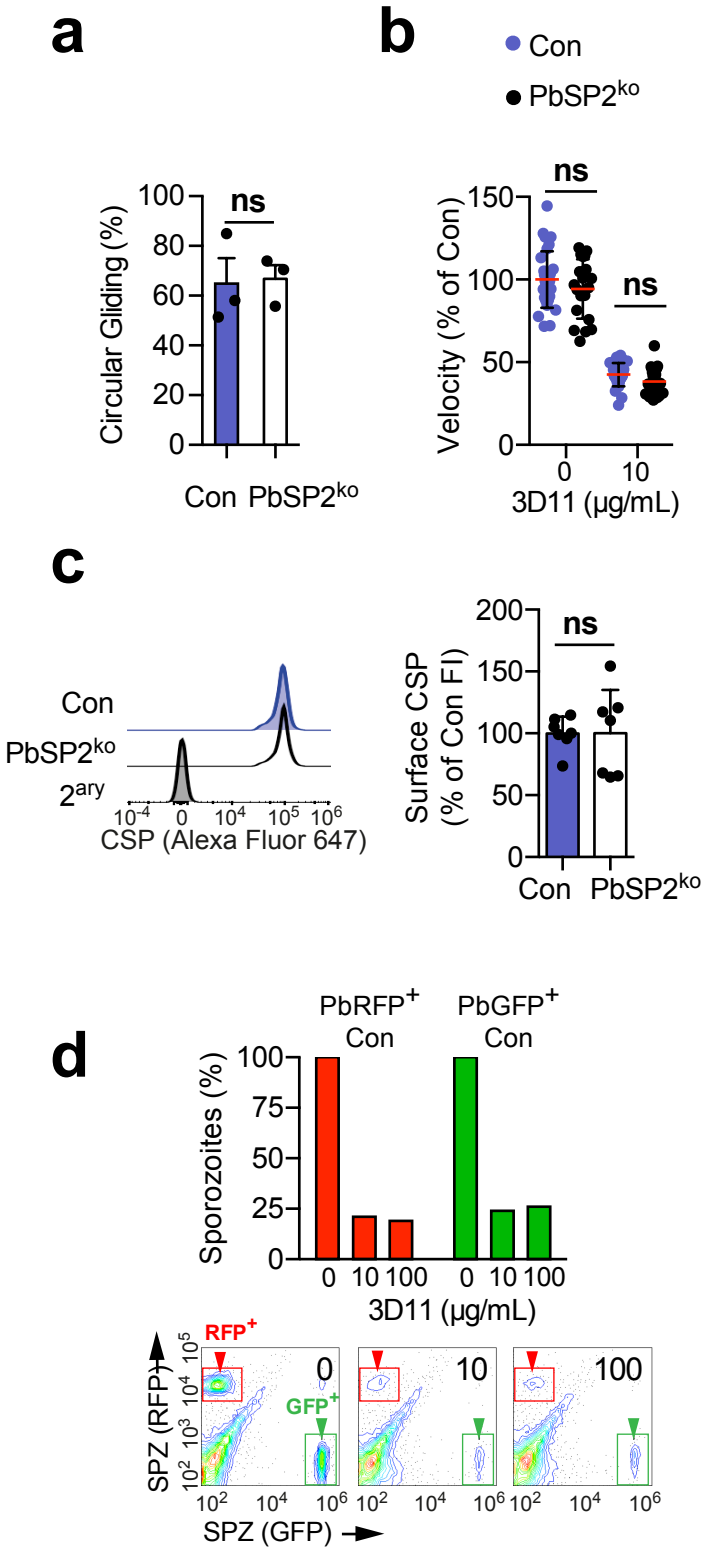
Figure S4. Aliprandini et al